Polymer Journal (2016) 48, 653–658
© 2016 The Society of Polymer Science, Japan (SPSJ) All rights reserved 0032-3896/16
www.nature.com/pj

ORIGINAL ARTICLE

Renaturation behavior of xanthan with high molar mass and wide molar mass distribution

Yasuhiro Matsuda, Fumitada Sugiura, Kazuya Okumura and Shigeru Tasaka

Light scattering and viscosity measurements were carried out for thermally renatured xanthan samples with various molar masses and molar mass distributions. The increases in the molar mass, radius of gyration and intrinsic viscosity of a xanthan sample with high molar mass and wide molar mass distribution upon renaturation were smaller than in xanthan samples with lower molar masses and narrower molar mass distributions. This behavior could be explained by the increase in 'intra-dimer renaturation' caused by the slower diffusion of xanthan with higher molar mass. The smaller change in the structure and viscosity of xanthan samples with higher molar mass and wider molar mass distribution may contribute to the stability of xanthan as a viscosity enhancer.
Polymer Journal (2016) **48,** 653–658; doi:10.1038/pj.2015.128; published online 27 January 2016

INTRODUCTION

Xanthan is a polysaccharide produced by *Xanthomonas campestris* and is widely used as a viscosity enhancer in foods, detergents, cosmetics and other products. It is widely accepted that native xanthan forms double helices, loses these helices upon heating under low ionic strength (denaturation) and recovers double helices upon cooling in solution under high ionic strength (renaturation).[1] Because products using xanthan are sometimes heated and cooled, for example during cooking, and the structural alterations affect the behavior of xanthan as a viscosity enhancer, the characterization of the structural change of xanthan attracts not only academic but also industrial interest.

There have been many studies on the structural changes in xanthan induced by thermal renaturation using light scattering,[2–5] optical rotation, circular dichroism (CD),[2–4,6] rheological measurements[2–4,6,7] and atomic force microscopy.[8,9] However, because the overall structure of renatured xanthan differs depending on the denaturation and renaturation conditions, such as the concentration of xanthan, ionic strength of solutions and temperatures, the structural alteration of xanthan induced by renaturation has not been elucidated clearly despite the number of studies.

We performed size exclusion chromatography-on line multi angle light scattering and CD measurements for xanthan samples with molar masses of $1.2–14 \times 10^5$ in their native state under different denaturation and renaturation conditions.[10] When the concentrations of xanthan and added salt for renaturation were not low, the molar mass and radius of gyration were higher than for the xanthan before the denaturation and renaturation, but the radius of gyration of the renatured xanthan was smaller than for native xanthan with the same molar mass. This experimental result suggests the formation of branched aggregates of xanthan, as schematically shown in Figure 1C. The structure as shown in Figure 1C was observed by atomic force microscopy (AFM), which supports the suggested structural change.[11]

To elucidate the structure of xanthan by light scattering or AFM, xanthan samples with lower molar mass are more convenient. Light scattering for samples with higher molecular weight requires data at smaller scattering angles because the linear region of scattering light is limited in smaller angles with an increase of the dimension and molar mass of a sample polymer. However, even tiny dust particles in sample solutions can spoil the data of light scattering, especially at small angles, which requires more severe purification of sample solutions for samples with higher molar masses. For AFM, longer chains of xanthan samples with higher molar mass make AFM images too complicated to characterize. Moreover, the complexity caused by molar mass distribution disturbs the clear analysis of both light scattering and AFM.

To avoid these difficulties in measurements and analysis, xanthan samples for our previous studies[10,11] were prepared by strong ultrasonic treatment followed by fractionation to decrease their molar mass and molar mass distribution. However, xanthan is used for industrial purposes without decreasing the molar mass and molar mass distribution because decreasing molar mass weakens the ability of xanthan as a viscosity enhancer, and the troublesome procedure to decrease molar mass distribution gives no useful characteristics as a viscosity enhancer.

In this study, we have tried to elucidate the structural change in a renatured xanthan sample without decreasing their molar mass and molar mass distribution by static light scattering and viscosity measurements. To estimate the influence of molar mass and molar mass distribution on the renaturation behavior, xanthan samples with different molar masses and molar mass distributions were also used for the measurements.

Department of Applied Chemistry and Biochemical Engineering, Shizuoka University, Shizuoka, Japan
Correspondence: Dr Y Matsuda, Department of Applied Chemistry and Biochemical Engineering, Shizuoka University, 3-5-1 Johoku, Naka-ku, Hamamatsu, 432-8561 Shizuoka, Japan.
E-mail: matsuda.yasuhiro@shizuoka.ac.jp
Received 22 July 2015; revised 6 December 2015; accepted 8 December 2015; published online 27 January 2016

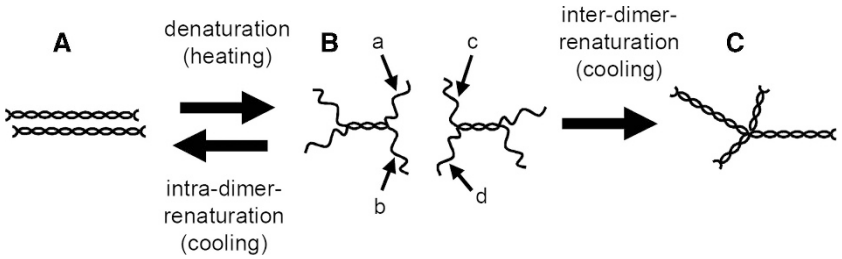

Figure 1 Schematic images of xanthan denatured and renatured under relatively high xanthan concentration proposed in our previous work.[10] The letters are used to explain the renaturation behavior in the text.

EXPERIMENTAL PROCEDURE

A xanthan sample purchased from Tokyo Kasei Kogyo (Tokyo, Japan) was used in this study as a sample without decreasing its molar mass and molar mass distribution. The lot number of the sample is B82UL-EL. In the following, this sample is designated as the 'NF' (not fractionated) sample. Four xanthan samples (S7-2, KC-2, KH1–3 and X15-2-3d) kindly provided by Professor Takahiro Sato at Osaka University, were used to estimate the influence of molar mass and molar mass distribution. These samples were prepared by sonication, purification, fractionation and neutralization, details of which are described in his previous report.[12] All the samples were dissolved in aqueous solution containing 0.01 M of sodium chloride, neutralized with dilute aqueous solutions of chloric acid and sodium hydroxide, and precipitated in acetone. This concentration of sodium chloride is enough to stabilize the double helices of xanthan at room temperature, because the melting temperature (T_M) of the double helices of xanthan is above 45 C° which can be calculated by equation (1). The precipitates were washed with aqueous solution containing 95 vol% acetone to remove sodium chloride, then washed with pure acetone to remove water and dried under vacuum for >72 h.

To estimate the influence of molar mass distribution, a xanthan sample with molar mass as high as KC-2 was prepared by mixing the S7-2 and KH1–3 samples. S7-2 and KH1–3 were separately dissolved in 0.1 M of sodium chloride (for native solution) or pure water (for renatured solution) and the two solutions were mixed (weight fraction of S7-1:KH1–3 = 81:100). In the following, this mixed sample is designated as 'Mix'.

To prepare 'native xanthan' solutions, dried samples were dissolved into aqueous solution containing 0.1 M of sodium chloride, and stirred for >24 h before measurements. 'Renatured xanthan' solutions were prepared as follows. First, dried xanthan samples were dissolved into water purified using a Millipore Direct-Q (Merck, Darmstadt, Germany) with an electric resistivity of about 18 MΩ cm. Solutions with a xanthan concentration of 0.01 g cm^{-3} were heated at 80 °C for an hour by immersing the solutions in a water bath of a NCB-1200 circulator temperature controller manufactured by Tokyo Rikakikai (Tokyo, Japan). After heating, sodium chloride was added to the solutions to obtain a sodium chloride concentration of 0.1 M. After stirring the solutions at room temperature for 24 h, they were diluted with aqueous solution containing 0.1 M sodium chloride to make xanthan concentrations suitable for the measurements.

The denaturation and renaturation behaviors of xanthan depend on the denaturation and renaturation conditions, especially the concentrations of xanthan and added salt, and some structural alterations other than the one shown in Figure 1 were also observed in our previous studies.[10,11] In this study, the denaturation and renaturation conditions were fixed, as described in the previous paragraph, to focus on the molar mass dependence of the structural alteration of xanthan. In our previous studies,[10,11] we have shown that xanthan forms branched aggregates as shown in Figure 1C under this condition. We are planning to investigate the concentration dependence of the structural alteration of xanthan by renaturation in our future work.

CD spectra were measured to estimate the change of double helices of xanthan samples induced by denaturation and renaturation with a JASCO J-720WO spectropolarimeter (Jasco, Hachioji, Japan). A quartz cell with 0.5 cm optical pass length was used and the temperature was controlled with a JASCO PTC-423L using a Peltier device (Jasco). Native and renatured samples were prepared as described in the previous paragraph. The solvent and measurement temperature were 0.1 M aqueous solution of sodium chloride, and 25 °C, respectively. Denatured solutions were prepared by dissolving xanthan samples into 0.01 M aqueous solution of sodium chloride or pure water, and measured at 80 °C. The xanthan concertation of all the samples was fixed to be 0.5 g l^{-1}.

Milas and Rinaudo[13] carried out optical rotation measurements for solutions with various concentrations of xanthan ($c_{xanthan}$) and NaCl (c_{NaCl}) at elevated temperatures, and T_M of the double helices of xanthan as a function of $c_{xanthan}$ and c_{NaCl}. If we use °C, g l^{-1}, and M as the units of T_M, $c_{xanthan}$, and c_{NaCl}, this function can be calculated as follows:

$$T_M = 45.8\log(c_{NaCl} + 1.03\times 10^{-3} c_{xanthan}) + 137 \quad (1)$$

By using equation (1), T_M of the solutions for denaturation for light scattering and viscosity measurements is 47 °C, and T_M of the solution with 0.01 M of sodium chloride and 0.5 g l^{-1} of xanthan, which was prepared for a CD measurement to estimate the denaturation condition was 46 °C. These are practically the same as that adopted by Liu *et al.*[2–4] (3 g l^{-1} of xanthan, and 0.01 M of sodium chloride, $T_M = 51$ °C). By using equation (1), T_M of xanthan in 0.01 M aqueous solution of sodium chloride is above 45 °C, which indicates that the double helices of xanthan are stable in 0.01 M aqueous solution of sodium chloride at room temperature.

Light scattering measurements were carried out with a DLS-7000 light scattering system manufactured by Otsuka Electronics (Hirakata, Japan), using a He-Ne laser with a wavelength of 633 nm as a light source. The long wavelength of the light source is suitable to determine the molar masses and radii of gyration of samples with high molar masses. Measurement cells with a diameter of 12 mm were manufactured by AGC Asahi Techno Glass (Yoshida-cho, Japan). The cells were rinsed with acetone filtered through hydrophilic PTFE filter units with a pore size of 0.20 μm and dried in a dustless desiccator before the measurements. Sample solutions were poured through hydrophilic PTFE filter units with a pore size of 0.45 μm. Toluene filtered through hydrophilic PTFE filter units with a pore size of 0.20 μm was used to calibrate the Rayleigh ratio (1.083×10^{-5} cm^{-1}). The scattering angles were chosen depending on the estimated size (radius of gyration) of the samples. The temperature was controlled at 25.0 °C by circulating water from the NCB-1200 circulator temperature controller (Tokyo Rikakikai).

Berry plots were adopted to calculate the weight average molar mass M_w and z-average radius of gyration $<S^2>_z^{1/2}$ from the data obtained for the samples with low molar masses (S7-2, KC-2, Mix and KH1–3). For the samples with high molar masses (NF and X15-2-3d), obtained data were extrapolated to zero concentration by Berry plots at first. Debye plots were adopted to extrapolate the data to zero angle to calculate M_w and $<S^2>_z^{1/2}$ using only the data from scattering angles small enough to obtain appropriate values of M_w and $<S^2>_z^{1/2}$.[10] The abscissa of a Debye plot is u, which is defined as $<S^2>^{1/2} k$, where k and $<S^2>^{1/2}$ indicate the magnitude of the scattering vector and radius of gyration, respectively. In a low k region, the dependence of the intensity of scattered light can be approximated as follows:

$$\frac{R_\theta}{\lim_{\theta\to 0} R_\theta} = \frac{2}{u^2}(e^{-u} + u - 1) \quad (2)$$

where R_θ indicates the excess Rayleigh ratio at scattering angle θ. The high limit of u suitable to obtain appropriate values of M_w and $<S^2>_z^{1/2}$ is shown in our previous paper.[10]

A conventional Ubbelohde type capillary viscometer manufactured by Asahi Glassplant (Arao, Japan) was used to obtain the intrinsic viscosities [η] of the samples with low molar masses. The temperature was controlled at 25.0 °C by immersing the viscometer in a TRW-27TP water bath manufactured by Tokyo Rikakikai.

To eliminate the influence of shear rate on the measured viscosities, a four-bulb spiral capillary viscometer[14,15] manufactured by Asahi Glassplant was used to determine the intrinsic viscosities of the samples with high molar masses. A four-bulb spiral capillary viscometer has a very long capillary (*ca.* 110 cm in our study) and four bulbs with different apparent shear rates $\dot{\gamma}$, which can be calculated as follows:[15]

$$\dot{\gamma} = \frac{h\rho g a}{2\eta l} \tag{3}$$

where h, ρ, g, a, η and l indicate the height from the midpoint of the upper and lower marks for each bulb to the meniscus of a liquid column, density of liquid, acceleration of gravity, radius of the capillary, viscosity of liquid and length of the capillary, respectively. The reduced viscosities for each solution were measured at finite shear rates, and extrapolated to a zero shear rate. The reduced viscosities at zero shear rate were analyzed in the same way as the data obtained using a conventional Ubbelohde type capillary viscometer.

SEC measurements were carried out to estimate the molar mass distributions of the native samples using 0.1 M NaCl aqueous solution as eluent. Two analysis columns (TSKgel $GMPW_{XL}$) and a guard column (TSKguardcolumn PW_{XL}) were connected directly to separate samples. The exclusion limit of the analysis columns was 5×10^7 for dextran. All the columns were products of Tosoh (Tokyo, Japan). The temperature of the columns was controlled at 40 °C. The eluent was flew at 0.5 ml min^{-1} with a Tosho HPLC-8020 system with a UV detector. The calibration curve was determined by using xanthan samples with low molar masses and narrow molar mass distribution. (S7-2, KC-2 and KH1–3) Because the M_w of these samples were determined by light scattering, the calibration curve was determined for their elution curves to give the same M_w determined by light scattering.

RESULTS AND DISCUSSION

Table 1 summarizes the M_w and molar mass distributions (M_w/M_n) of the samples used in this study. The M_w of all the samples and M_w/M_n of the samples with low M_w were determined successfully, but measurements for M_w/M_n of the samples with high M_w were difficult. The elusion curves for NF and X15-2-3d were very asymmetric. One of the reasons is tailing because xanthan, especially with high M_w, enhances the viscosity of its solution drastically. Moreover, because xanthan with high M_w has a very large dimension, NF and X15-2-3d seem to contain molecules over the exclusion of the columns. For these reasons, we gave up obtaining accurate values of M_w/M_n for NF and X15-2-3d.

Figure 2 summarizes CD spectra of NF and S7-2 with the lowest molar mass in this study. No distinct difference could be detected between the spectra of NF and S7-2, which indicates the change of double helical structure of xanthan samples with high molar mass and wide molar mass distribution was essentially identical to that of xanthan samples with lower molar mass and narrower molar mass distribution. There were also no distinct difference between the spectra of native and renatured xanthan, whereas the negative peak around 225 nm was shifted to shorter wavelength and the intensity of the positive peak around 205 nm decreased by the denaturation in water and 0.01 M aqueous solution of sodium chloride. These results were consistent with those in our previous paper[10], and indicate that the double helices of xanthan were unwound by the denaturation, and rewound by renaturation irrespective of the molar mass of xanthan sample.

Figure 3 shows typical results of light scattering for native and renatured xanthan with low molar mass (KH-1–3). The open and filled circles indicate measured and extrapolated data, respectively. The

Table 1 Molar masses and molar mass distributions of xanthan samples at the native state

Sample	$M_{w,na}/10^5$	$(M_w/M_n)_{na}$
S7-2	2.53[a]	1.1[b]
KC-2	4.85[a]	1.3[b]
Mix	5.08[a]	1.6[c]
KH1–3	6.71[a]	1.4[b]
NF	45.2[a]	~2[d]
X15-2-3d	64.5[a]	~2[d]

[a]Determined by light scattering.
[b]Determined by an ordinary SEC curve.
[c]Calculated by the molar mass distributions of KC-2 and KH-1–3 and the mixing ratio.
[d]Estimated by a SEC curve affected by tailing and the exclusion limit of the columns.

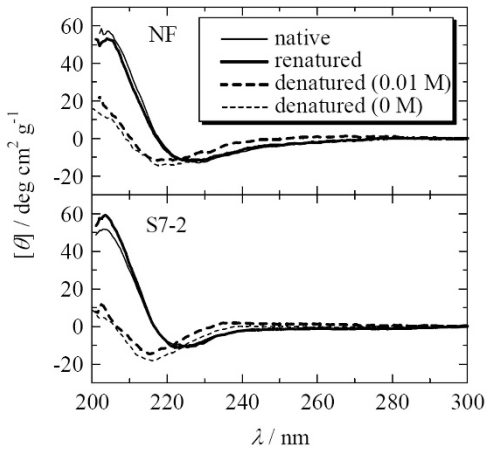

Figure 2 Circular dichroism spectra of native, renatured and denatured xanthan samples. The numbers in parentheses indicate the molar concentration of sodium chloride. The details of solution preparation are described in the text.

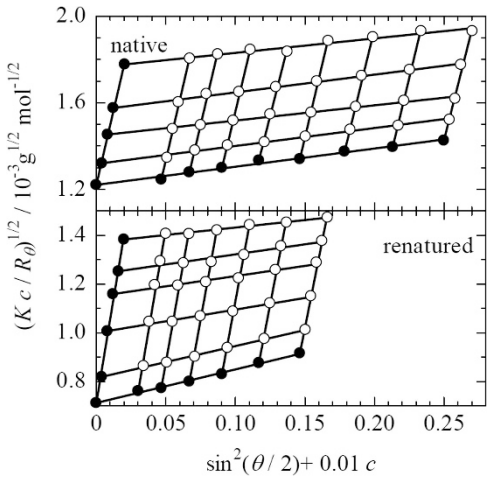

Figure 3 Typical results of light scattering for native and renatured xanthan with low molar mass (KH-1–3). Open and filled circles indicate measured and extrapolated data points, respectively. Solid lines were used to extrapolate the data to zero concentration or zero scattering angle. The unit of c is g l^{-1}.

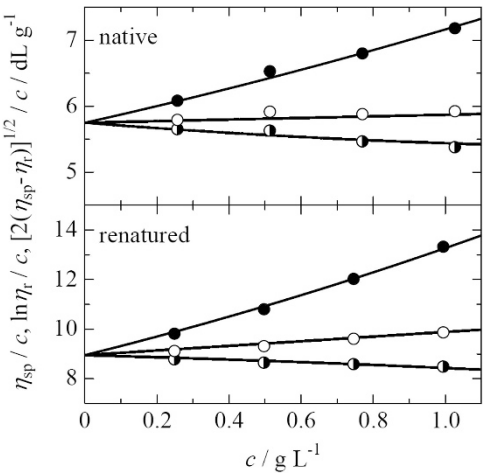

Figure 4 Typical results of viscosity measurements for native and renatured xanthan with low molar mass (KH-1–3). Filled, half-filled and open circles indicate Huggins, Mead–Fuoss and Billmeyer plots, respectively. Solid lines were used to extrapolate the data to zero concentration.

solid lines used to extrapolate the data to zero concentration or zero scattering angle well fit the open circles, which shows that the data were successfully extrapolated to obtain M_w and $<S^2>_z^{1/2}$.

Figure 4 shows typical results of viscosity measurements for native and renatured xanthan of KH-1–3. Filled, half-filled and open circles indicate Huggins, Mead–Fuoss and Billmeyer plots, respectively. Solid lines were used to extrapolate the data to zero concentration, and the lines fit the circles well.

The results of light scattering for the native and renatured NF samples are shown in Figure 5. The data points are shifted vertically with α shown in the figure to make the data points clear. The measured data in Figure 5a were extrapolated to infinite dilution, and the intercepts were plotted in Figure 5b to extrapolate to zero angle. The solid lines in Figure 5b were calculated by equation (2) and fit the data points well.

Figure 6 summarizes the results for the viscosity measurements for the native and renatured NF. The data points in Figure 6a are vertically shifted with α shown in the figure to make the data points clear. The reduced viscosities at finite shear rates can be smoothly extrapolated to a zero shear rate as shown in Figure 6a, and intrinsic viscosities were successfully obtained using these data with appropriate Huggins coefficients.

The light scattering and viscosity measurements for the other samples were also performed successfully. The Huggins coefficients k' obtained by viscosity measurements in this study were 0.3–0.6. It is well known that k' is 0.3–0.6 for most polymers including xanthan, and higher values of k' are sometimes caused by the dissociation of aggregates during dilution in viscosity measurements. The obtained values of k' support the absence of such dissociation for the xanthan samples used in this study.

The molar mass dependences of $<S^2>_z^{1/2}$ and $[\eta]$ are shown in Figure 7. The open and filled symbols indicate the data for native and renatured samples, respectively, and the data points with different shapes indicate the data for different xanthan samples. The solid and broken lines in the figure indicate the molar mass dependence of $<S^2>_z^{1/2}$ and $[\eta]$ determined by Sato *et al.*[12,16,17] for native xanthan samples with various M_w and narrow molar mass distribution using the wormlike chains model for $<S^2>_z^{1/2}$ and the touched bead wormlike model for $[\eta]$ to best fit their experimental data. They used

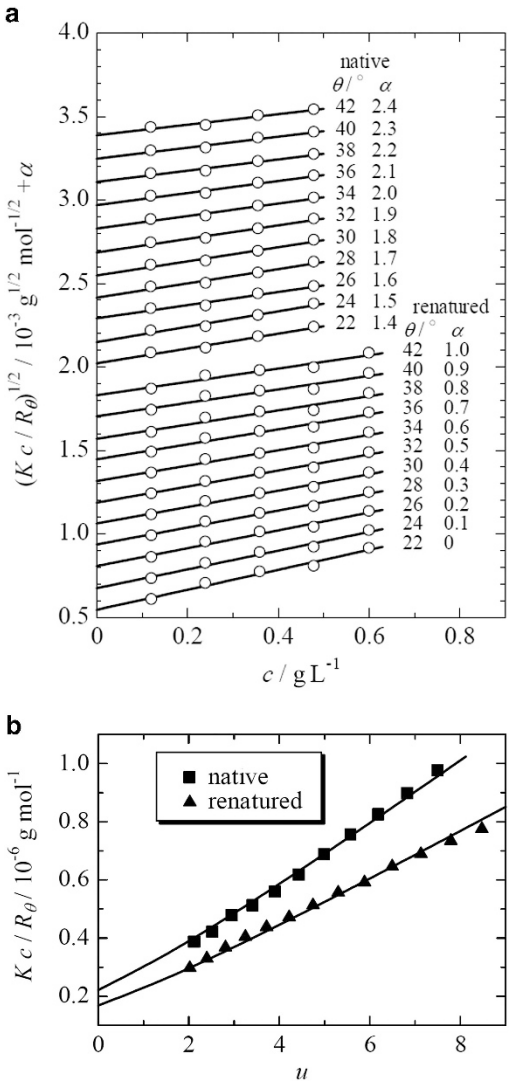

Figure 5 Typical results of light scattering for native and renatured xanthan with high molar mass (NF). First, measured data were extrapolated to zero concentration as shown in **a**, and the data extrapolated to zero concentration were extrapolated to zero angle in Debye plots as shown in **b**. The data points in **a** are vertically shifted with α shown in the figure to make the data points clear. Solid lines in **b** were calculated using equation (2).

120 nm and 1940 nm^{-1} for persistence length (q) and molar mass per contour length (M_L) to calculate $<S^2>_z^{1/2}$ and $q = 100$ nm, $M_L = 1940$ nm^{-1} and bead diameter (d) of 2.2 nm to calculate $[\eta]$. In our previous work[10], the molar mass dependence of $<S^2>_z^{1/2}$ were measured by SEC-MALS, and the obtained data can be fitted by using $q = 100$ nm, $M_L = 1940$ nm^{-1}. The deviation of q determined by Sato *et al.*[12,16,17] might be caused by the slightly wide molar mass distribution of their samples, especially those with high M_w.

Although the M_w, $<S^2>_z^{1/2}$, and $[\eta]$ were increased by renaturation, the $<S^2>_z^{1/2}$ and $[\eta]$ of the renatured xanthan were smaller than for native xanthan with the same M_w. The smaller $<S^2>_z^{1/2}$ and $[\eta]$ of renatured xanthan compared with the values of native xanthan with the same M_w were also measured in our previous work.[10] Because the CD spectrum of renatured xanthan indicates that the local chiral structure (double helices) of renatured xanthan is almost identical to that of native xanthan, the smaller $<S^2>_z^{1/2}$ and $[\eta]$ of renatured xanthan were attributed to the branched structure of renatured

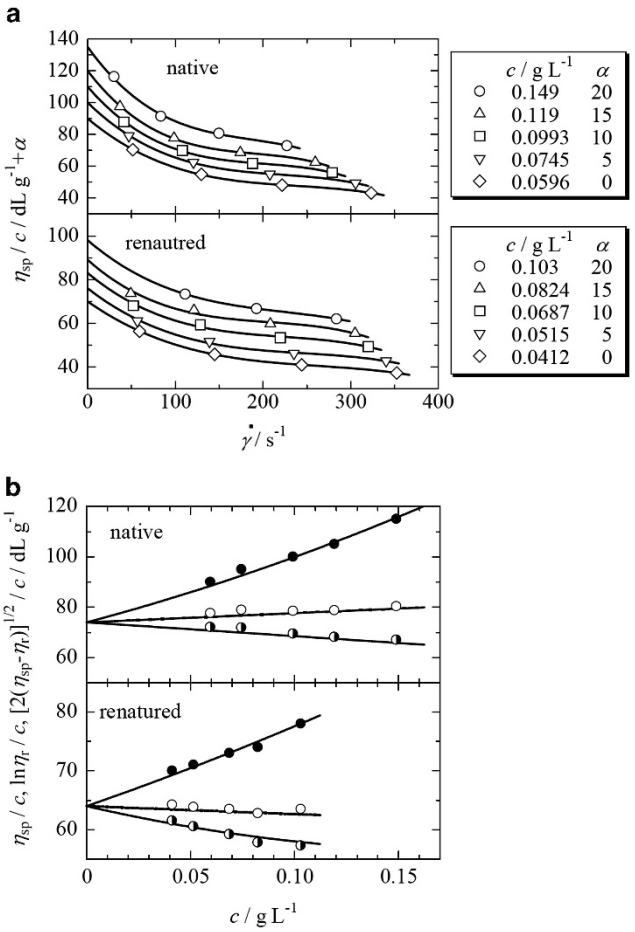

Figure 6 Typical results of viscosity measurements for native and renatured xanthan with high molar mass (NF): (**a**) shear rate dependence of the viscosity of each solution, (**b**) viscosity of each solution at zero shear rate. The data points in **a** are vertically shifted with α shown in the figure to make the data points clear. Filled, half-filled and open circles in **b** indicate Huggins, Mead–Fuoss and Billmeyer plots, respectively.

xanthan. AFM observations of renatured xanthan also support the existence of its branched structure.[11]

Figure 7 also indicates that the increases in M_w, $<S^2>_z^{1/2}$, and $[\eta]$ induced by the renaturation were more drastic for xanthan samples with lower M_w. To show the molar mass dependence of the increase of these physical properties, the ratios of M_w, $<S^2>_z^{1/2}$, and $[\eta]$ of renatured xanthan to the corresponding physical properties of native xanthan were plotted against M_w of native xanthan as shown in Figure 8. The subscripts 're' and 'na' indicate renatured and native, respectively. Figure 8 clearly shows that the ratios decreased drastically about 5×10^5.

The smaller increases in M_w, $<S^2>_z^{1/2}$, and $[\eta]$ induced by renaturation for xanthan samples with higher molar mass can be explained by a hypothesis that the unwound chain length was shorter for xanthan samples with higher M_w, but the CD spectra shown in Figure 2 denied this hypothesis.

Liu *et al.*[2–4] also carried out optical rotation measurements for xanthan samples with M_w of $0.585–25.0\times10^5$. Their denaturation conditions were different from those in this study, but T_M calculated by equation (1) was almost same as ours. They showed that the absolute value of the optical rotation at 80 °C increase with an increase of M_w below 1.04×10^5, but it was independent from M_w above

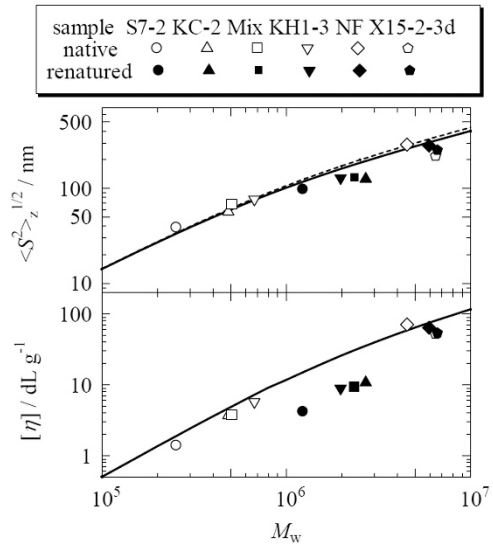

Figure 7 Molar mass dependence of radii of gyration, and intrinsic viscosities of native and renatured xanthan samples. The lines are calculated by the wormlike chain model (for radius of gyration) and the touched bead wormlike chain model (for intrinsic viscosity) for native xanthan. The solid and broken curves for radius of gyration were calculated using $q=100$ nm and $M_L=1940$ nm^{-1} and $q=120$ nm and $M_L=1940$ nm^{-1}, respectively. The curve for intrinsic viscosity was calculated using $q=100$ nm, $M_L=1940$ nm^{-1} and $d=2.2$ nm.

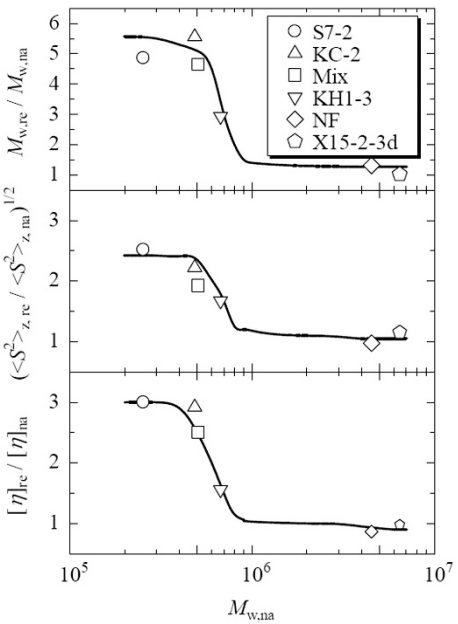

Figure 8 Ratios of molar mass, radius of gyration and intrinsic viscosity of renatured xanthan to the corresponding values for native xanthan. The solid lines are shown for eye guide. The subscripts 'na' and 're' indicate the physical properties of the native and renatured samples, respectively.

2.07×10^5. This result denies the hypothesis described in the previous paragraph.

The aggregation behaviors of polymers can be changed below and over the overlap concentration (c^*) defined as follows with Avogadro's

number, N_A:

$$c^* \equiv \frac{3M}{4\pi N_A \langle S^2 \rangle^{3/2}} \quad (4)$$

Because c^* decreases with an increase of molar mass, the molar mass dependence of the renaturation behavior shown in Figure 8 can be affected if the xanthan concentration at renaturation was below c^* for the samples with low M_w, and above c^* for the samples with high M_w. Liu *et al.* [2–4] carried out light scattering measurements for denatured xanthan, and reported $<S^2>_z^{1/2}$ was 32 nm for the xanthan with M_w of 2.07×10^5. These values give c^* of 8.4×10^{-4} g cm^{-3}, which indicates that the xanthan concentration in this study (0.01 g cm^{-3}) is higher than c^* for all the samples.

Considering the discussion mentioned above, we propose a model which can qualitatively explain the renaturation behavior shown in Figure 8 as follows. The double helices of a xanthan dimer partially unwind by heating (A → B in Figure 1) and rewind by cooling at the xanthan concentration in this study. During the renaturation process, two dimers can form an aggregate with a double molar mass (B → C) if double helices rewind between two unwound coils belonging to two different dimers (between coils a and c, and between coils b and d). In the following, such renaturation is termed 'inter-dimer renaturation'. However, if double helices rewind between unwound coils belonging to the same dimers (between coils a and b, and between coils c and d), xanthan dimers recover almost same structure they had before the denaturation. (B → A). In the following, such renaturation is termed 'intra-dimer renaturation'. Although inter-dimer renaturation induces the increase in M_w, $<S^2>_z^{1/2}$, and $[\eta]$, these physical properties show no distinct changes upon intra-dimer renaturation. For inter-dimer renaturation, an unwound coil must encounter another unwound coil belonging to another dimer before it rewinds a double helix with an unwound coil belonging to the same dimer. Because dimers with higher molar mass have lower transitional diffusion coefficients (in other words, higher hydrodynamic radii), intra-dimer renaturation is more favorable than inter-dimer renaturation for xanthan samples with higher molar mass.

The molar mass at which intra-dimer renaturation becomes more favorable than inter-dimer renaturation may depend on the concentration of xanthan. However, the concentration of xanthan affects not only the frequency of xanthan dimers to encounter another dimer but also the denaturation and renaturation behaviors of xanthan, such as the rate of residual double helix at the denaturation.[10,13] For this reason, even if experiments are conducted for xanthan denatured and renatured at different concentrations, it will be difficult to eliminate the influence of the frequency of xanthan dimers to encounter another dimer from the experimental data.

To elucidate the influence of molar mass distribution on the renaturation behavior, the Mix sample was prepared by mixing S7-2 and KH1–3 samples to adjust its M_w to the same value as KC-2. However, no distinct difference was observed between the renaturation behaviors of the Mix and KC-2 samples, and their renaturation behaviors can be described by the curves in Figure 7, which suggests that renaturation behavior is determined by the molar mass of a xanthan sample. This result suggests that not the molar mass distribution but the molar mass of a xanthan sample dominates the renaturation behavior, although the molar mass distribution can affect the renaturation behavior.

CONCLUSION

A commercially available xanthan sample with high molar mass and wide molar mass distribution was denatured by heating, then renatured by cooling under the condition that induces xanthan to form branched aggregates upon renaturation. The results of light scattering and viscosity measurements indicated the existence of branched aggregates for the commercially available xanthan sample, but the increase in the molar mass, radius of gyration and intrinsic viscosity of this sample were smaller than for xanthan samples with lower molar masses and narrower molar distributions. The ratios of molar mass, radius of gyration and intrinsic viscosity of renatured xanthan to the values for native xanthan decreased with an increase of the molar mass of native xanthan. This molar mass dependence of the renaturation behavior can be explained by a model that intra-dimer renaturation is more favorable than inter-dimer renaturation for xanthan samples with higher molar mass. The smaller change in the structure and viscosity of commercially available xanthan with high molar mass and wide molar mass distribution may contribute to its stability as a viscosity enhancer.

CONFLICT OF INTEREST

The authors declare no conflict of interest.

ACKNOWLEDGEMENTS

We thank Professor Takahiro Sato at the Department of Macromolecular Science, Osaka University who kindly provided the xanthan samples, allowed us to use the light scattering and CD instruments and advised us about the viscosity measurements using the four-bulb spiral capillary viscometer. This work is partially supported by a grant from The Japan Health Foundation.

1 Norisuye, T. & Teramoto, A. in *Polymeric Materials Encyclopedia* (ed. Salamone J. C.) 8801–8809 (CRC Press, Boca Raton, USA, 1996).
2 Liu, W., Sato, T., Norisuye, T. & Fujita, H. Thermally induced conformational change of xanthan in 0.01 M aqueous sodium chloride. *Carbohydr. Res.* **160**, 267–281 (1987).
3 Liu, W. & Norisuye, T. Order-disorder conformation change of xanthan in 0.01 M aqueous sodium chloride: dimensional behavior. *Biopolymers* **27**, 1641–1654 (1988).
4 Liu, W. & Norisuye, T. Thermally induced conformation change of xanthan: interpretation of viscosity behavior in 0.01 M aqueous sodium chloride. *Int. J. Biol. Macromol.* **10**, 44–50 (1988).
5 Capron, G., Brigand, G. & Muller, G. About the native and renatuerd conformation of xanthan exopolysaccharide. *Polymer* **38**, 5289–5295 (1997).
6 Kawakami, K., Okabe, Y. & Norisuye, T. Dissociation of dimerized xanthan in aqueous solution. *Carbohydr. Polym.* **14**, 189–203 (1991).
7 Oviatt, H. W. Jr. & Brant, D. A. Viscoelastic behavior of thermally treated aqueous xanthan solutions in the semidilute concentration regime. *Macromolecules* **27**, 2402–2408 (1994).
8 Camesano, T. A. & Wilkinson, K. J. Single molecule study of xanthan conformation using atomic force microscopy. *Biomacromolecules* **2**, 1184–1191 (2001).
9 Ikeda, S., Gohtani, S., Nishinari, K. & Zhong, Q. Single molecules and networks of xanthan gum probed by atomic force microscopy. *Food Sci. Technol. Res.* **18**, 741–745 (2012).
10 Matsuda, Y., Bjiyajima, Y. & Sato, T. Thermal denaturation, renaturation, and aggregation of a double-helical polysaccharide xanthan in aqueous solutions. *Polym. J.* **41**, 526–532 (2009).
11 Matsuda, Y., Sugiura, F., Mays, J. W. & Tasaka, S. Atomic force microscopy of thermally renatured xanthan with low molar mass. *Polym. J.* **47**, 282–285 (2015).
12 Sato, T., Norisuye, T. & Fujita, H. Double-stranded helix of xanthan in dilute solution: evidence from light scattering. *Polym. J.* **16**, 341–350 (1984).
13 Milas, M. & Rinaudo, M. Conformational investigation on the bacterial polysaccharide xanthan. *Carbohydr. Res.* **76**, 189–196 (1979).
14 Larkins, J. H., Perrings, J. D., Shepherd, G. R. & Nland, B. J. An automatic recording multigradient capillary viscometer. *J. Chem. Educ.* **42**, 555–556 (1965).
15 Einaga, Y., Miyaki, Y. & Fujita, H. Intrinsic viscosity of polystyrene. *J. Polym. Sci. Polym. Phys. Ed.* **17**, 2103–2109 (1979).
16 Sato, T., Kojima, S., Norisuye, T. & Fujita, H. Double-stranded helix of xanthan in dilute solution: further evidence. *Polym. J.* **16**, 423–429 (1984).
17 Sato, T., Norisuye, T. & Fujita, H. Double-stranded helix of xanthan in dilute solution: dimensional and hydrodynamic properties in 0.1 M aqueous sodium chloride. *Macromolecules* **17**, 2696–2700 (1984).